Ground-based optical atomic clocks as a tool to monitor vertical surface motion

Bondarescu, Ruxandra ; Schärer, Andreas ; Lundgren, Andrew ; Hetényi, György ; Houlié, Nicolas ; Jetzer, Philippe ; Bondarescu, Mihai

DOI: https://doi.org/10.1093/gji/ggv246

Geophysical Journal International

Geophys. J. Int. (2015) **202,** 1770–1774
GJI Gravity, geodesy and tides

doi: 10.1093/gji/ggv246

EXPRESS LETTER

Ground-based optical atomic clocks as a tool to monitor vertical surface motion

Ruxandra Bondarescu,[1] Andreas Schärer,[1] Andrew Lundgren,[2] György Hetényi,[3,4] Nicolas Houlié,[4,5] Philippe Jetzer[1] and Mihai Bondarescu[6,7]

[1]*Department of Physics, University of Zürich, Switzerland. E-mail: ruxandra@physik.uzh.ch*
[2]*Albert Einstein Institute, Hannover, Germany*
[3]*Swiss Seismological Service, ETH Zürich, Switzerland*
[4]*Department of Earth Sciences, ETH Zürich, Switzerland*
[5]*Department of Civil, Environmental and Geomatic Engineering, ETH Zürich, Switzerland*
[6]*Department of Physics and Astronomy, University of Mississippi, Oxford, MS, USA*
[7]*Facultatea de fizica, Universitatea de Vest, Timisoara, Romania*

Accepted 2015 June 8. Received 2015 June 5; in original form 2015 April 21

SUMMARY

According to general relativity, a clock experiencing a shift in the gravitational potential ΔU will measure a frequency change given by $\Delta f/f \approx \Delta U/c^2$. The best clocks are optical clocks. After about 7 hr of integration they reach stabilities of $\Delta f/f \sim 10^{-18}$ and can be used to detect changes in the gravitational potential that correspond to vertical displacements of the centimetre level. At this level of performance, ground-based atomic clock networks emerge as a tool that is complementary to existing technology for monitoring a wide range of geophysical processes by directly measuring changes in the gravitational potential. Vertical changes of the clock's position due to magmatic, post-seismic or tidal deformations can result in measurable variations in the clock tick rate. We illustrate the geopotential change arising due to an inflating magma chamber using the Mogi model and apply it to the Etna volcano. Its effect on an observer on the Earth's surface can be divided into two different terms: one purely due to uplift (free-air gradient) and one due to the redistribution of matter. Thus, with the centimetre-level precision of current clocks it is already possible to monitor volcanoes. The matter redistribution term is estimated to be 3 orders of magnitude smaller than the uplift term. Additionally, clocks can be compared over distances of thousands of kilometres over short periods of time, which improves our ability to monitor periodic effects with long wavelength like the solid Earth tide.

Key words: Transient deformation; Gravity anomalies and Earth structure; Geopotential theory; Tides and planetary waves.

1 INTRODUCTION

Vertical deformation transients are key to characterizing many geological processes such as magmatic or tectonic deformation (Fig. 1). Many of these processes have timescales from hours to years which are difficult to measure with existing instruments. Atomic clocks provide a new tool to resolve vertical displacement, with a current precision of about 1 cm in equivalent height after an integration time of 7 hr (Bloom *et al.* 2014).

In the past, we argued (Bondarescu *et al.* 2012) that clocks provide the most direct local measurement of the geoid, which is the equipotential surface (constant clock tick rate) that extends the mean sea level to continents. Since a clock network is ground-based, it can provide variable spatial resolution and can be used to calibrate and add detail to satellite maps, which suffer from aliasing (errors due to effects faster than the sampling rate) and from the attenuation of the gravitational field at the location of the satellite.

In this paper, we consider dynamic sources that cause both vertical displacement and underground mass redistribution which produce changes in the local geopotential. Geopotential differences ΔU are directly measured by the changes in clock tick rate $\Delta f/f \approx \Delta U/c^2$, where c is the speed of light. To be useful, a clock must always be compared to a reference clock, which could be nearby or thousands of kilometres away. Clocks are connected via ultraprecise fiber links that are capable of disseminating their frequency signals over thousands of kilometres with a stability beyond that of the clock (Droste *et al.* 2013). As a concrete example we present the case of the inflation (or deflation) of an underground magma chamber, computed analytically (Mogi 1958), and apply it to the Etna volcano. We explore whether the magma filling

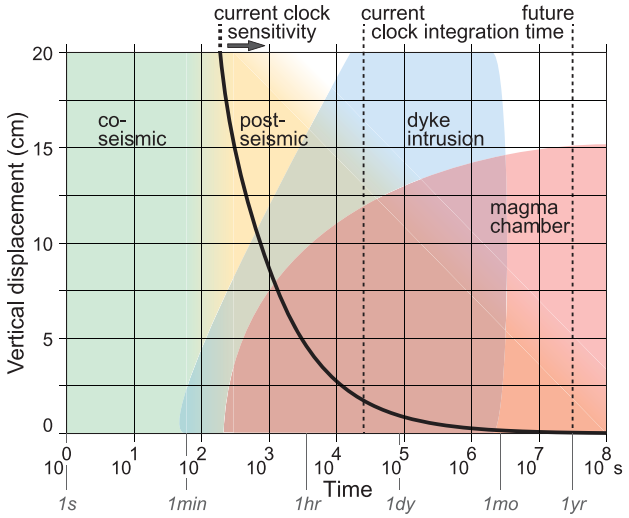

Figure 1. Phenomena that could be monitored with optical clock networks. The black line shows the lower sensitivity of today's best optical clocks; see eq. (1) and Δz_{today} in eq. (7). The vertical dashed lines show current and planned clock integration times.

could be detected using one or two clocks located on the volcanic edifice.

The primary tools currently used to monitor vertical displacement are Interferometric Synthetic Aperture Radar (InSAR) and GPS. InSAR measures millimetre displacements in the line of sight of radar satellites over wide areas (e.g. Bürgmann *et al.* 2000; Biggs *et al.* 2011), but with limited sampling rates (days to weeks). GPS is able to measure vertical displacements of 1 cm over short timescales ($\sim$ 1 hr) only when the displacement is very localized in the network and/or the frequency of motion is different from the frequency of various artefacts that impact GPS accuracy. After surveying areas for more than 10 yr, the level of accuracy of GPS techniques is close to the millimetre level (Blewitt & Lavallée 2002; Houlié & Stern 2012) or better, enabling us to better characterize the crustal elastic contrast of plate boundaries (Jolivet *et al.* 2009; Houlié & Romanowicz 2011). Since the primary source of noise in GPS measurements is due to signal dispersion through the atmosphere, both differential GPS and post-processed GPS data perform better if networks are dense (e.g. Khan *et al.* 2010; Houlié *et al.* 2014) because many artefacts cancel across networks over which the ionosphere and troposphere can be assumed to be constant. For timescales of seconds, broad-band seismometers can be used (Houlié & Montagner 2007), but their bandwidth is unsuited for resolving long-term displacements (Boore 2003).

Unlike the GPS or InSAR measurements, local atomic clock measurements are insensitive to atmospheric perturbations, and could resolve ground displacement over shorter integration timescales (hours to months). Further, clocks in conjunction with gravimeters are also able to resolve density changes in the Earth crust that do not, or just partially, lead to uplift or subsidence. In the case of a spherical magma chamber, the geopotential term resulting from mass redistribution is inversely proportional to the distance to the source $\sim 1/R$, whereas the ground displacement term scales with $1/R^2$. As opposed to this, both terms have the same $1/R^2$ scaling in gravity surveys. Comparing the measured gravity change to the uplift, $\Delta g/\Delta h$, can reduce this degeneracy to model processes a volcano is undergoing before eruption (Rymer & Williams-Jones 2000) and also more general processes (see Fig. 1 and De Linage *et al.* 2007).

Even in areas without active seismic or volcanic processes, the solid Earth tide has a vertical amplitude that can be as high as 30 cm (Agnew 2007) with a semi-diurnal period, whose amplitude can be monitored by an atomic clock that is compared with a distant reference clock. We find that geopotential and gravity measurements are sensitive to two different combinations of tidal Love numbers, and could be used to calibrate existing measurements of the solid Earth tide.

2 OVERVIEW OF ATOMIC CLOCKS

According to Einstein's theory of general relativity, time slows down in the vicinity of massive objects. On a neutron star, clocks tick at about half their rates on Earth. An observer outside the horizon of a black hole even sees time stopping all together at the horizon. Similarly, clocks that are closer to Earth tick slightly slower than clocks that are further away.

Atomic clocks employ atomic transitions that are classified, depending on the transition frequency, as either microwave or optical clocks. Since the clock frequency depends only on a known atomic transition and constants of nature, clocks respond identically to changes in the gravitational potential and do not require calibration. This is in contrast to relative gravimeters, which suffer from instrument drift and have to be calibrated via comparisons with other measurements at the same location. The current definition of the second is based on a microwave atomic clock. However, optical clocks have the potential for higher stability because they utilize atomic transitions with resonance line-widths typically 10^5 narrower than microwave transitions. Since the development of the femtosecond laser frequency comb, optical clocks have been improving extremely rapidly (Poli *et al.* 2014). Today's best clocks are optical. They are laboratory devices with frequency uncertainty

$$\Delta f/f \sim 3 \times 10^{-16}/\sqrt{\tau/\text{s}}, \tag{1}$$

where τ is the integration period (Hinkley *et al.* 2013; Bloom *et al.* 2014), and are likely to continue to improve dramatically within the next decade (Poli *et al.* 2014). A transportable optical clock that monitors and compensates for environmental effects (temperature, pressure, electric and magnetic fields) and fits within two cubic meters has recently been built (Poli *et al.* 2014).

In the future, it is expected that clocks will become sensitive to surface displacements at the sub-millimetre level. Possible techniques include nuclear optical transitions (Campbell *et al.* 2012), optical transitions in Erbium (Kozlov *et al.* 2013), and transitions in highly charged ions (Derevianko *et al.* 2012). A stability of

$$\Delta f/f \sim \sigma_{\text{tomorrow}} = 10^{-17}/\sqrt{\tau/\text{s}} \tag{2}$$

should be possible (Hinkley *et al.* 2013), which would achieve $\Delta f/f \sim 10^{-20}$ within one month.

In order to take full advantage of the improved stability of optical clocks, distant clocks have to be compared reliably to the 10^{-18} level. This entails a global understanding of vertical displacements, the solid Earth tide, and, overall, of the geoid to the 1-cm level. Any effects that cause perturbations to this level would have to be reliably modelled and understood. Clock comparisons via satellites are currently limited by the precision of the communication link that passes through a potentially turbulent atmosphere. The most precise comparisons of distant clocks currently use underground optical fiber links. Optical frequency transfer with stability better than the clock has been demonstrated over a two-way distance of 1840 km (Droste *et al.* 2013), with a fiber-link from Braunschweig, Germany to Paris, France. A fiber-link network capable of

disseminating ultrastable frequency signals is being planned throughout Europe (e.g. NEAT-FT collaboration, REFIMEVE+).

3 METHODS

While clocks are sensitive to changes in the gravitational potential, relative gravimeters see changes in the vertical component of the gravitational acceleration, which is a vector ($\vec{g} = -\vec{\nabla}U$) whose amplitude can generally be measured much better than its direction. They both provide local measurements of the change in gravity or potential relative to a reference point where the gravity and potential are known accurately. Within a large fiber links network, the reference clock could be very far away.

For a displacement z, the geopotential and gravity changes are

$$\Delta U \approx -\frac{GM_\oplus}{R_\oplus^2} z, \quad \Delta g \approx \frac{2GM_\oplus}{R_\oplus^3} z. \tag{3}$$

where G is the gravitational constant, and $M_\oplus$ and $R_\oplus$ the mass and radius of the Earth. The well-known free-air correction Δg for gravity is the gradient of the potential change ΔU.

A vertical displacement of $z = 1$ cm causes changes in the geopotential and in gravity of

$$\Delta U \approx 0.1 \left(\frac{z}{1\ \mathrm{cm}}\right) \frac{\mathrm{m}^2}{\mathrm{s}^2}, \tag{4}$$

$$\Delta g \approx 3 \times 10^{-8} \left(\frac{z}{1\ \mathrm{cm}}\right) \frac{\mathrm{m}}{\mathrm{s}^2} \sim 3 \left(\frac{z}{1\ \mathrm{cm}}\right) \mu\mathrm{Gal}. \tag{5}$$

Thus, the frequency of a clock changes by

$$\frac{\Delta f}{f} \approx \frac{\Delta U}{c^2} \sim 10^{-18} \left(\frac{z}{1\ \mathrm{cm}}\right). \tag{6}$$

The solid line in Fig. 1 is the vertical displacement $\Delta z_{\mathrm{today}}$ as a function of clock integration time τ, which is obtained by equating eqs (1) and (6), while $\Delta z_{\mathrm{tomorrow}}$ results from eqs (2) and (6).

$$\Delta z_{\mathrm{today}} \approx 300 \left(\frac{\tau}{\mathrm{s}}\right)^{-1/2} \mathrm{cm}, \quad \Delta z_{\mathrm{tomorrow}} \approx 10 \left(\frac{\tau}{\mathrm{s}}\right)^{-1/2} \mathrm{cm}. \tag{7}$$

4 APPLICATIONS

We first discuss the geopotential and gravity changes caused by an inflating magma chamber, using the Mogi model. This is followed by a discussion of the measurability of the solid Earth tides.

4.1 Inflating magma chamber—the Mogi model

An inflating or deflating magma chamber can be described by the so-called 'Mogi model' (Mogi 1958): an isolated point pressure source in an elastic half-space that undergoes a pressure change. The Mogi model is broadly used in the literature (e.g. Houlié *et al.* 2006; Biggs *et al.* 2011). Recently, its predictions were compared to sophisticated simulations, which showed that in many situations the discrepancy is quite small (Pascal *et al.* 2014).

Clocks and gravimeters lying above the magma chamber will be affected by (1) a ground displacement, (2) the change of mass density within the chamber, (3) the uplifted rock and (4) the change in the density of the surrounding material. We refer to effects (2), (3) and (4) as 'mass redistribution' (ΔU_2, ΔU_3 and ΔU_4 in Appendix A in supplementary material). The change of the gravitational potential due to ground displacement (1) arises since the observer is shifted to a position farther away from the centre of the Earth. A Mogi source centred at $(0, d)$ that undergoes a volume change ΔV deforms the half-space, lifting an observer sitting at $(r, 0)$ by

$$|w| = (1-\nu)\frac{\Delta V}{\pi} \frac{d}{(r^2+d^2)^{3/2}}, \tag{8}$$

where ν is Poisson's ratio. For crustal rock the typical value is $\nu \approx 0.25$. Using eq. (3) with $z = w$, this uplift changes the potential by

$$\Delta U_1 \approx -\frac{GM_\oplus}{R_\oplus^2} w = \frac{GM_\oplus}{R_\oplus^2}(1-\nu)\frac{\Delta V}{\pi} \frac{d}{(r^2+d^2)^{3/2}}, \tag{9}$$

where higher order terms have been neglected. When we add the contribution of the mass redistribution terms

$$\Delta U_{\mathrm{m}} = G\rho_m \Delta V \frac{1}{\sqrt{r^2+d^2}}. \tag{10}$$

The total geopotential change is

$$\begin{aligned} \Delta U &= \Delta U_1 + \Delta U_{\mathrm{m}} \\ &= \frac{GM_\oplus}{R_\oplus^2}(1-\nu)\frac{\Delta V}{\pi} \frac{d}{(r^2+d^2)^{3/2}} + G\rho_m \Delta V \frac{1}{\sqrt{r^2+d^2}}, \end{aligned} \tag{11}$$

where ρ_m is the magma density. Typically, the change due to mass redistribuiton ΔU_{m} is several orders of magnitude smaller than that due to uplift ΔU_1. Measuring the mass redistribution term would require that we subtract the uplift term which may be obtained individually using other techniques like GPS or InSAR.

Similarly, the change in the gravitational acceleration is given by

$$\begin{aligned} \Delta g &= \Delta g_1 + \Delta g_m \\ &= \left[-\frac{2GM_\oplus}{R_\oplus^3}\frac{1-\nu}{\pi} + G\rho_m\right] \Delta V \frac{d}{(r^2+d^2)^{3/2}}. \end{aligned} \tag{12}$$

Note that for both the acceleration and the potential the different terms of (2), (3) and (4) mostly cancel each other and only a term $\sim\rho_m$ survives (see Appendix A supplementary material for the complete calculation). However, this cancellation is a consequence of the elastic half-space assumption of the Mogi model and will be less exact in more realistic scenarios. On the one hand, for the acceleration all terms have the same spatial dependence. On the other hand, for the potential they scale differently: while the uplift term scales as d/R^3 like all acceleration terms, the mass redistribution term scales as $1/R$, where $R = \sqrt{r^2+d^2}$ is the distance to the source.

Assuming a clock with stability $\Delta f/f = \sigma_0/\sqrt{\tau/\mathrm{s}}$ and a source with a constant volume change rate $\Delta V/\Delta\tau$, the minimum required integration time to measure the uplift at a location (r, d)

$$\tau_1 = \left[\frac{\sigma_0 \pi c^2}{g(1-\nu)} \frac{R^3}{d} \left(\frac{\Delta V}{\Delta\tau}\right)^{-1} \mathrm{s}^{-1}\right]^{2/3} \mathrm{s}, \tag{13}$$

with $g = GM_\oplus/R_\oplus^2$, whereas for the mass redistribution

$$\tau_m = \left[\frac{\sigma_0 R c^2}{G\rho_m} \left(\frac{\Delta V}{\Delta\tau}\right)^{-1} \mathrm{s}^{-1}\right]^{2/3} \mathrm{s}. \tag{14}$$

We focus on the specific example of the Etna volcano. Houlié *et al.* (2006) used GPS data to investigate its underground magma system and found that a Mogi source located about 9.5 km below the summit with a volume change rate of $30 \times 10^6\ \mathrm{m^3 yr^{-1}}$ would yield the observed uplift. In Fig. 2, we plot the ground motion and the resulting potential change as well as the potential change due to mass redistribution. We find that $\Delta U_m \sim 10^{-3}\Delta U_1$, which roughly

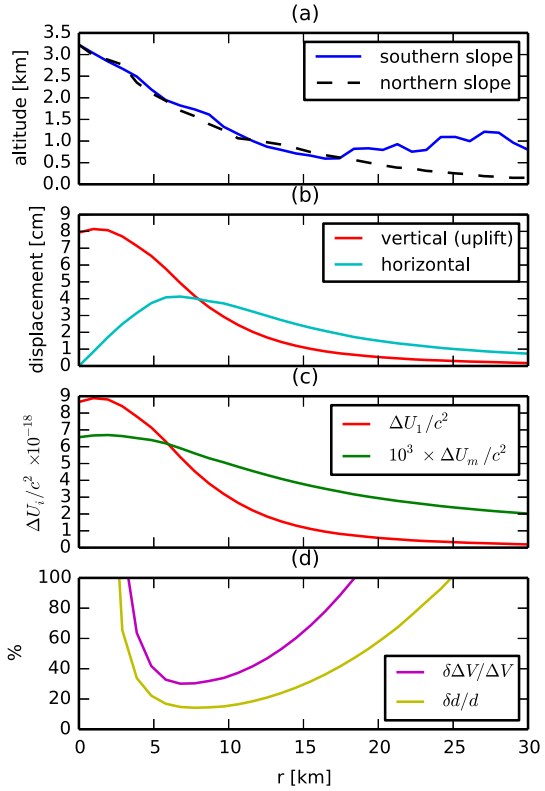

Figure 2. Estimate of vertical ground deformation on the Etna volcano over the course of 1 yr with the Mogi model. In (a), the altitude profile of Etna is shown. The solid curve shows the southern slope of the mountain, the dashed line shows the mirror image of the northern slope. For the following plots only the former is considered since the latter gives very similar results. Assuming a Mogi source located 9.5 km below the summit with a volume change rate of 30×10^6 m^3 yr^{-1}, the vertical and horizontal motion over 1 yr is plotted in (b). The change in the gravitational potential due to this uplift together with the change due to mass redistribution is shown in (c). Notice that the latter is about 3 orders of magnitude smaller. If one clock is positioned at the summit, (d) shows the fractional errors on the measurements of the source depth $\delta d/d$ and the volume change $\delta\Delta V/V$ as a function of the horizontal distance to a second clock.

corresponds to $\Delta f/f \sim \Delta U/c^2 \sim 10^{-20}$. If we assume constant volume change rate, an optical clock on the summit would see the uplift if integrated for about ten days (eq. 13), while the mass redistribution signal is out of reach. With a clock stability σ_{tomorrow}, such an uplift would be observable within a day, and the mass redistribution in five months.

We also give an example of how to best choose the clock locations. We assume that the horizontal position of the magma chamber is already known from previous surveys, and that the two measurements we wish to make are the depth of the magma chamber d and the volume change ΔV (assuming also that ν is known). With one clock directly above the magma chamber, we find the location of a second clock which minimizes the measurement errors on d and ΔV; of course there must also be a distant reference clock. For a flat half-space we find the optimal location to be at a horizontal distance $r \approx 0.78d$ (note that the minima is broad; see Appendix A5 in supplementary material). Assuming Etna to be a half-space with chamber depth 9.5 km, the fractional errors there are $\delta d/d \approx 18$ per cent and $\delta\Delta V/\Delta V \approx 38$ per cent. Including the height profile of the mountain, Fig. 2(d) shows $\delta d/d$ and $\delta\Delta V/\Delta V$ as a function of the distance to the summit, assuming a clock sensitive to $\Delta U/c^2 = 10^{-18}$. We find that the optimal location of a second clock is $r \approx 0.78\,d$, independent of the clock's performance. For the performance considered here, this corresponds to $\delta d/d \approx 14$ per cent and $\delta\Delta V/\Delta V \approx 30$ per cent.

4.2 Solid Earth tides

Solid Earth tides are the deformation of the Earth by the gravitational fields of external bodies, chiefly the Moon and the Sun. In general relativity the Earth is freely falling, so at the centre of the Earth the external gravitational force is cancelled by the Earth's acceleration towards the external body. Because the external field is not uniform, other points experience a position-dependent tidal force (Agnew 2007).

The tide has three effects of concern on the gravitational potential. First is the external potential itself, which can be calculated directly from the known mass and position of the external bodies. Second is the change in the Earth's gravitational potential produced by the deformation of the Earth. Third is the vertical displacement of the surface, which produces a free-air correction to our measurements. The last two effects are proportional to the first, parameterized by the Love numbers k_n and h_n, respectively (Agnew 2007).

As shown in Appendix B supplementary material, clocks (sensitive to geopotential changes) and gravimeters (sensitive to the downward component of g) each measure a different linear combination of the Love numbers. This is because the three effects scale differently with the distance from the centre of the Earth. It is therefore desirable to combine gravimeter and clock measurements to infer the Love numbers with great accuracy. Recall that clock measurements must be made between a pair of clocks. Since tidal effects are global, both clocks are sensitive to the tidal deformation; one clock cannot simply be treated as a reference. To measure the tidal amplitude, it is necessary to compare instruments over distances of the order of half the tidal wavelength on timescales shorter than the period of the tide. The tidal wavelength is half the circumference of the Earth for the dominant tidal mode. Both differential GPS and InSAR have short baseline, so tidal effects are small and are mostly subtracted by modelling. A network of clocks where each clock pair is separated by hundreds of kilometres could more holistically monitor solid Earth tides. Current clocks provide measurements of the vertical uplift to within a percent of the maximal tidal amplitude on an hourly basis. Such measurements could be used to monitor stress changes within the crust, and to investigate whether these correlate with triggered seismicity.

Such a network of clocks on the continent scale could accurately measure the tidal Love numbers. The external tidal potential can be decomposed into a sum of Legendre polynomials

$$U^n_{\text{tid}}(R,\alpha) = -\frac{GM_{\text{ext}}}{R}\left(\frac{R_\oplus}{R}\right)^n P_n(\cos\alpha), \tag{15}$$

where R is the distance between the external body of mass M_{ext} and the Earth's centre of mass, and α is the angle from the observation point to the line between the centre of the Earth and the external body. Since $R_\oplus/R \approx 1/60$ for the Moon, and $R_\oplus/R \approx 1/23\,000$ for the Sun, it is typically sufficient to just consider the first few terms of the expansion. By linearity, we treat each n separately.

The potential change measured by a clock, including all three effects above, is

$$\Delta U_n = (1 + k_n - h_n)U^n_{\text{tid}}(R,\alpha). \tag{16}$$

The change in the vertical gravitational acceleration measured by a gravimeter is

$$\Delta g_n = -n\left(1 - \frac{n+1}{n}k_n + \frac{2}{n}h_n\right)\frac{U^n_{\text{tid}}(R,\alpha)}{R_\oplus}. \tag{17}$$

Combining the two measurements with the known $U^n_{\rm tid}(R_\oplus, \alpha)$ we can determine the Love numbers

$$k_n = \frac{n+2}{n-1} + \frac{R_\oplus \Delta g_n - 2\Delta U_n}{(n-1)U^n_{\rm tid}(R_\oplus, \alpha)}, \quad (18)$$

$$h_n = \frac{2n+1}{n-1} + \frac{R_\oplus \Delta g_n - (n+1)\Delta U_n}{(n-1)U^n_{\rm tid}(R_\oplus, \alpha)}. \quad (19)$$

Both Love numbers are believed to be modelled to within a fraction of a percent (Yuan & Chao 2012). These models will be tested throughly once a global optical clock network becomes available.

5 CONCLUSIONS

We have demonstrated the promise of very precise atomic clocks for geophysical measurements with two illustrative examples. In the inflation or deflation of a spherical magma chamber (the Mogi model), clocks are primarily sensitive to the local vertical displacement resulting at the Earth's surface. Such monitoring of local deformations can be done using a reference clock anywhere outside the zone where the displacement is significant, typically tens of kilometres. However, when monitoring solid Earth tides, the best accuracy will be obtained with a clock network spanning the globe.

Beyond the examples given, it should be possible to use clocks in conjunction with gravimeters to monitor dyke intrusion, post-seismic deformation, aquifer variations, and other effects causing vertical displacement or subsurface mass change. In contrast to GPS and InSAR measurements, ground clock measurements are insensitive to the turbulence in the atmosphere.

In the future, optical clocks are expected to become part of the global ground-clock network that is used for telecommunications increasing the precision with which we can monitor time. Ground clocks can thus be combined with existing instrumentations (GPS, InSAR, gravimeters) to track underground mass redistribution through its effects on the geopotential. Portable optical clocks have already been developed (Poli *et al.* 2014), and could monitor changes in the geopotential of the Earth across fault lines, in areas with active volcanoes, and for surveying.

REFERENCES

Agnew, D.C., 2007. *Treatise on Geophysics, 3.06 - Earth Tides,* Elsevier, pp. 163–195.

Biggs, J., Bastow, I.D., Keir, D. & Lewi, E., 2011. Pulses of deformation reveal frequently recurring shallow magmatic activity beneath the Main Ethiopian Rift, *Geochem. Geophys. Geosyst.,* **12,** Q0AB10, doi:10.1029/2011GC003662.

Blewitt, G. & Lavallée, D., 2002. Effect of annual signals on geodetic velocity, *J. geophys. Res.,* **107**(B7), 2145, doi:10.1029/2001JB000570.

Bloom, B.J. *et al.*, 2014. An optical lattice clock with accuracy and stability at the 10^{-18} level, *Nature,* **506,** 71–75.

Bondarescu, R., Bondarescu, M., Hetényi, G., Boschi, L., Jetzer, P. & Balakrishna, J., 2012. Geophysical applicability of atomic clocks: direct continental geoid mapping, *Geophys. J. Int.,* **191,** 78–82.

Boore, D.M., 2003. Analog-to-digital conversion as a source of drifts in displacements derived from digital recordings of ground acceleration, *Bull. seism. Soc. Am.,* **93,** 2017—2024.

Bürgmann, R., Rosen, P.A. & Fielding, E.J., 2000. Synthetic aperture radar interferometry to measure earths surface topography and its deformation, *Annu. Rev. Earth Planet. Sci.,* **28,** 169–209.

Campbell, C.J., Radnaev, A.G., Kuzmich, A., Dzuba, V.A., Flambaum, V.V. & Derevianko, A., 2012. Single-ion nuclear clock for metrology at the 19th decimal place, *Phys. Rev. Lett.,* **108,** 120802, doi:10.1103/PhysRevLett.108.120802.

De Linage, C., Hinderer, J. & Rogister, Y., 2007. A search for the ratio between gravity variation and vertical displacement due to a surface load, *Geophys. J. Int.,* **171,** 986–994.

Derevianko, A., Dzuba, V.A. & Flambaum, V.V., 2012. Highly charged ions as a basis of optical atomic clockwork of exceptional accuracy, *Phys. Rev. Lett.,* **109,** 180801, doi:10.1103/PhysRevLett.109.180801.

Droste, S., Ozimek, F., Udem, Th., Predehl, K., Hnsch, T.W., Schnatz, H., Grosche, G. & Holzwarth, R., 2013. Optical-frequency transfer over a single-span 1840 km fiber link, *Phys. Rev. Lett.,* **111,** 110801, doi:10.1103/PhysRevLett.111.110801.

Hinkley, N. *et al.*, 2013. An Atomic Clock with 10^{-18} Instability, *Science,* **341,** 1215–1218.

Houlié, N. & Montagner, J.P., 2007. Hidden dykes detected on ultra long period seismic signals at Piton de la Fournaise volcano?, *EPSL,* **261,** 1–8.

Houlié, N. & Romanowicz, B., 2011. Asymmetric deformation across the San Francisco Bay Area faults from GPS observations in Northern California, *Phys. Earth planet. Inter.,* **184,** 143–153.

Houlié, N. & Stern, T., 2012. A comparison of GPS solutions for strain and SKS fast directions: implications for modes of shear in the mantle of a plate boundary zone, *EPSL,* **345–348,** 117–125.

Houlié, N., Briole, P., Bonforte, A. & Puglisi, G., 2006. Large scale ground deformation of Etna observed by GPS between 1994 and 2001, *Geophys. Res. Lett.,* **33,** L02309, doi:10.1029/2005GL024414.

Houlié, N., Dreger, D. & Kim, A., 2014. GPS source solution of the 2004 Parkfield earthquake, *Sci. Rep.,* **4,** 3646, doi:10.1038/srep03646.

Jolivet, R., Bürgmann, R. & Houlié, N., 2009. Geodetic exploration of the elastic properties across and within the northern San Andreas Fault zone, *Earth planet. Sci. Lett.,* **288,** 26–131.

Khan, S.A., Liu, L., Wahr, J., Howat, I., Joughin, I., van Dam, T. & Fleming, K., 2010. GPS measurements of crustal uplift near Jakobshavn Isbræ due to glacial ice mass loss, *J. geophys. Res.,* **115,** B09405, doi:10.1029/2010JB007490.

Kozlov, A., Dzuba, V.A. & Flambaum, V.V., 2013. Prospects of building optical atomic clocks using Er i or Er iii, *Phys. Rev. A,* **88,** 032509, doi:10.1103/PhysRevA.88.032509.

Mogi, K., 1958. Relations between eruptions of various volcanoes and the deformation of the ground surfaces around them, *Bull. Earthq. Res. Inst.,* **36,** 99–134.

Pascal, K., Neuberg, J. & Rivalta, E., 2014. On precisely modelling surface deformation due to interacting magma chambers and dykes, *Geophys. J. Int.,* **196,** 253–278.

Poli, N., Schioppo, M., Vogt, S., Falke, St., Sterr, U., Lisdat, Ch. & Tino, G.M., 2014. A transportable strontium optical lattice clock, *Appl. Phys. B,* **117,** 1107–1116.

Poli, N., Oates, C.W., Gill, P. & Tino, G.M., 2014. Optical atomic clocks, arXiv:1401.2378.

Rymer, H. & Williams-Jones, G., 2000. Volcanic eruption prediction: magma chamber physics from gravity and deformation measurements, *Geophys. Res. Lett.,* **27,** 2389–2392.

Yuan, L. & Chao, B.F., 2012. Analysis of tidal signals in surface displacement measured by a dense continuous GPS array, *EPSL,* **355,** 255–261.

SUPPORTING INFORMATION

Additional Supporting Information may be found in the online version of this paper:

Appendix (http://gji.oxfordjournals.org/lookup/suppl/doi:10.1093/gji/ggv246/-/DC1).

Please note: Oxford University Press is not responsible for the content or functionality of any supporting materials supplied by the authors. Any queries (other than missing material) should be directed to the corresponding author for the paper.